Effects of microstructure on very-high-cycle fatigue crack initiation and life scatter for a high strength steel

Zhengqiang Lei, Jijia Xie, Sun Chengqi, Xiaolong Liu, Youshi Hong*

State Key Laboratory of Nonlinear Mechanics, Institute of Mechanics, Chinese Academy of Sciences, Beijing 100190, PR China
* Corresponding author: hongys@imech.ac.cn

Abstract A type of high strength steel was tempered at 150℃, 180℃, and 300℃ to form three groups of specimens, and rotating bending fatigue tests were performed to investigate the effects of microstructure on the behavior of very-high-cycle fatigue (VHCF) crack initiation. With the increase of tempering temperature, S-N curves for the three specimen groups show a tendency of increasing life scatter and the threshold value of VHCF crack initiation ΔK_{FGA} decreases. For 150℃ tempered specimens, grain boundary initiation is dominant for fatigue crack initiation while inclusion initiation is dominant for the other two groups. Effects of inclusion and retained austenite on fatigue crack initiation are discussed, and reliability analysis based on Tanaka-Mura model is carried out to characterize VHCF life scatter.

Keywords Very-high-cycle fatigue, FGA, life scatter, inclusion

1. Introduction

It is well known that S-N curve of ferrous materials tends to a limit between 106 and 10^7 cycles of loading. This fatigue limit was true until the fatigue failure beyond 10^7 cycles was first reported in 1980s [1]. Afterwards various types of materials [2] were confirmed to failure after 10^7 loading cycles which was named as very-high-cycle fatigue (VHCF) [3]. S-N curves for high strength steels including VHCF regime often presents a step-wise tendency (duplex S-N curves [4]), and it provides a challenge for safety design of industrial structures or components. Especially for aircrafts, automobiles, ship, railways which need to enduring long period of cyclic loading up to 10^{10} cycles, there is an urgent necessity to clarify the behavior and mechanism of VHCF failures.

In low cycle fatigue (LCF) and high cycle fatigue (HCF) regime, fatigue cracks often originate from defects at the specimen surface, and fatigue crack propagation is dominant in fatigue failure. When stress is below the conventional fatigue limit, these defects may become non-propagating cracks [5], and the interior defects such as non-metallic inclusions acting as stress raisers become fatigue crack origin in VHCF regime [6]. Sometimes the prior austenite grains boundary could also be a crack origin for high-carbon chromium steel under low tempering temperature [7]. Meanwhile fatigue crack initiation is dominated for HCF and VHCF, and first few microstructure barriers control fatigue limit and scatter of lifetime. However, fatigue cracks grow in elastic-plastic field with less microstructure influence for LCF [8]. Studies on VHCF mechanism have shown that the great role of microstructures influence on interior fatigue crack initiation as the fine granular area (FGA [4]) presents. The influencing factors include spherical carbide [9], hydrogen [10], inclusion size [11], chemical compositions of inclusion [12]. The portions of life attributed to subsurface crack initiation in FGA are beyond 90% [13], thus all these microstructures which can influence the formation of FGA are reasonable for life scatters of VHCF.

Primary inclusions are often dominant sites of fatigue crack formation and early growth in high

strength steels, powder metallurgy alloys, and casting alloys. Transition from surface-dominated fatigue processes to subsurface failure initiation is often observed in these systems in moving from the LCF to the VHCF regime. Competition between near surface and bulk inclusions is said to be key to this failure mode transition, and introduces the large scatter of S-N curves [8]. Many studies on fatigue crack propagation have shown that fatigue crack growth behavior near threshold differs with the change of tempering temperature [14; 15; 16], i.e. the threshold value of crack growth ΔK_{th} varied with different heat treatment conditions.

In this paper, a type of high strength steel was tempered at 150℃, 180℃, and 300℃, to obtain three groups of specimens, and rotary bending fatigue tests were performed with them to investigate the influence of tempering temperature on S-N curve scatter properties from LCF regime to VHCF regime. And effects of microstructure on fatigue crack initiation and growth are discussed.

2. Experimental procedure

The test material in the present investigation is a high carbon chromium bearing steels with main chemical compositions (wt. %) of: 1.06 C, 1.04 Cr, 0.88 Mn, 0.34 Si, 0.027 P, and 0.005 S (Fe balance). From the spheroidizing annealed material, specimens were machined into hourglass shape providing a certain amount of finishing allowance. The specimens were heated at 845℃ for 2 hours in vacuum, then oil-quenched and tempered for 2 hours in vacuum at 150℃, 180℃ and 300℃. Such heat-treated specimens are of the microstructure with tempered martensite, retained austenite, and carbides, and the volume fractions of retained austenite are about 15%, 8% and 0 for 150℃, 180℃, and 300℃ tempered specimens respectively by means of X-ray diffraction (Fig. 1). Mechanical properties of three groups of specimens are shown in Table 1.

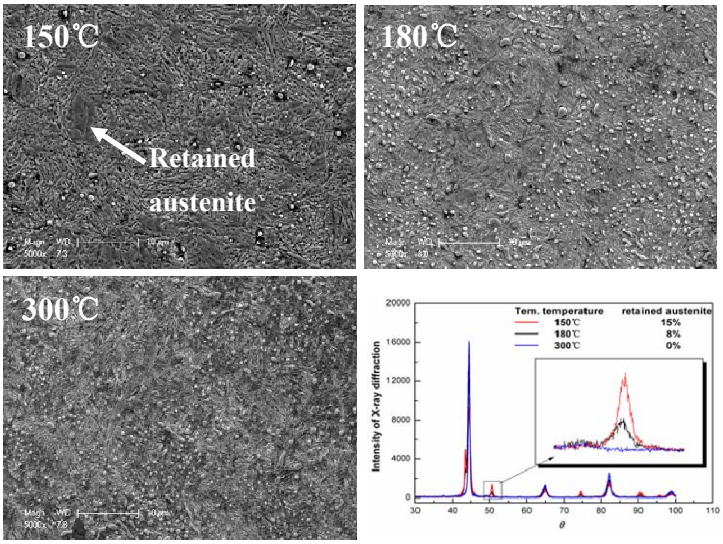

Fig. 1. The content of retained austenite for the specimens tempered at 150℃, 180℃ and 300℃ by means of X-ray diffraction.

The three specimen groups are denoted as RL150, RL180, and RL300 and their mechanical properties are shown in Table 1.

Table 1. Mechanical properties of three groups of specimens

Specimens group	Tempering Temp. (℃)	Micro-Hardness Hv (kgf/mm^2)	Tensile Stress σ_b
RL150	150	808	2163
RL180	180	753	1849
RL300	300	666	1690

Rotary bending tests were performed by using a "Giga-Quad" machine at room temperature with the frequency of 52.5 Hz and the stress ratio of -1. After the fatigue testing, the fracture surfaces of all fractured specimens were observed using a field-emission type scanning electron microscope (SEM). The geometries of specimens are shown in Fig. 2. The round notch surface was ground by the grade 400, 800, 1500 and 2000 abrasive papers and polished to a smooth finish.

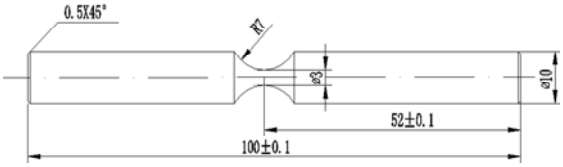

Fig. 2. Schematic drawing of the specimens (dimensions in mm).

3. S-N curves

Fig. 3 shows S-N curves of RL150, RL180, and RL300. It is seen that the shape of the S-N curve differed from each other for the three groups. For RL150, the S-N data almost locate at a straight line as the black line shows. The shape of S-N curves of RL180 presents a duplex stepwise tendency as one of the VHCF specific characteristics for metallic materials [4]. The S-N data scattered around two independent lines for RL300, resulting the uncertainty of fatigue life at a given stress level. For example, fatigue failures occurred at 10^4, 10^6, 10^7, 10^8 cycles when the maximum stress was about 700MPa. Meanwhile the increasing tendency of S-N curve as the decreasing of stress in VHCF regime is more obvious for RL300. The changes of the shape of S-N curves at different tempered temperature lead to a distinguishing scatter properties for the three groups of specimens. Comparing these S-N curves in Fig. 3, we can see an increasing tendency of life scatter as the tempering temperature increases from 150℃, 180℃ to 300℃.

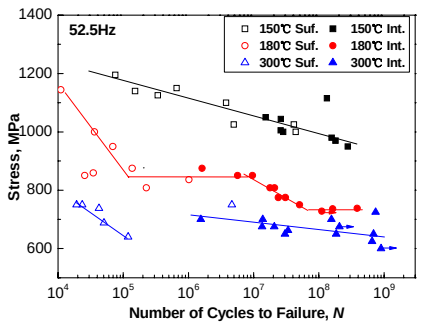

Fig. 3. S-N curves of 150℃, 180℃, and 300℃ tempered specimens under rotary bending loading. (Sur.: surface initiation, Int.: interior initiation)

4. Fracture surface observation

4.1 Characters of fracture surface

Fig. 4 shows the diminishing of the inter/trans granular zone in the fracture surface with the increase of the tempering temperature. The rough surface zone of region A outside of the fisheye (Fig. 4d) is considered as inter/trans granular zone by Zhao et al. [7]. Region A is clearly seen in the fracture surface of RL150 (Fig. 4a), while this zone diminishes gradually with the increase of the tempering temperature as Fig. 4b and Fig. 4c show. Under cyclic loading, materials with high brittleness is lack of sufficient number of independent slip systems to accommodate plastic deformation between contiguous grain leading to grain boundaries crack. Elevating of the tempering temperature can reduce its brittleness resulting the diminishing of inter granular fracture surface. This phenomenon also verifies the change of the microstructure with different heat treatments.

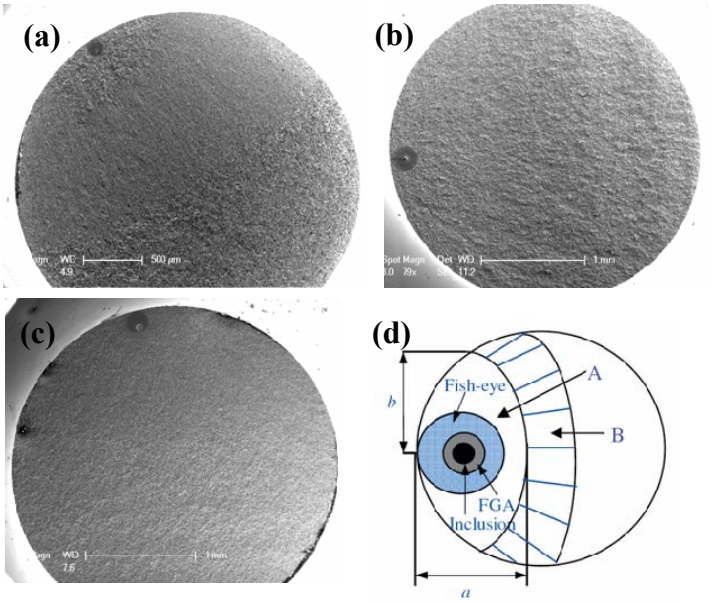

Fig. 4. Diminishing of the inter/trans granular zone with the increase of the tempering temperature: (a) RL150, (b) RL180, (c) RL300, and (d) Schematic drawing of the fracture surface (A denotes the inter/trans granular zone, and B denotes the fast growth zone).

4.2 Fatigue crack initiation

Fig. 5 shows the typical morphology of the fatigue crack origin for surface and interior initiation. For RL150, fatigue crack tends to initiate from the grains boundaries for VHCF as shown in Fig. 5a and Fig. 5b. Sometimes FGA was observed when the VHCF crack initiated from interior grains boundaries (Fig. 5b), and the proportion of grain boundary initiation is up to 88%. For RL180 and RL300, almost all VHCF failures originate from interior inclusions with a fisheye pattern as Fig. 5c shows. Fig. 5d shows an example of non-propagating cracks for surface inclusion. The size and the stress intensity factor (SIF) range are 29 μm and 3.65 MPa·$m^{1/2}$ for the subsurface inclusion, while they are 11 μm and 3.28 MPa·$m^{1/2}$ for the smaller one at the specimen surface. SIFs for both the two inclusion fall below the threshold value (5.0 MPa·$m^{1/2}$) for this heat treatment, and fatigue crack originates from the subsurface inclusion with higher SIF which indicates that SIF is an

key factor influencing fatigue crack initiation between surface inclusion and interior inclusion.

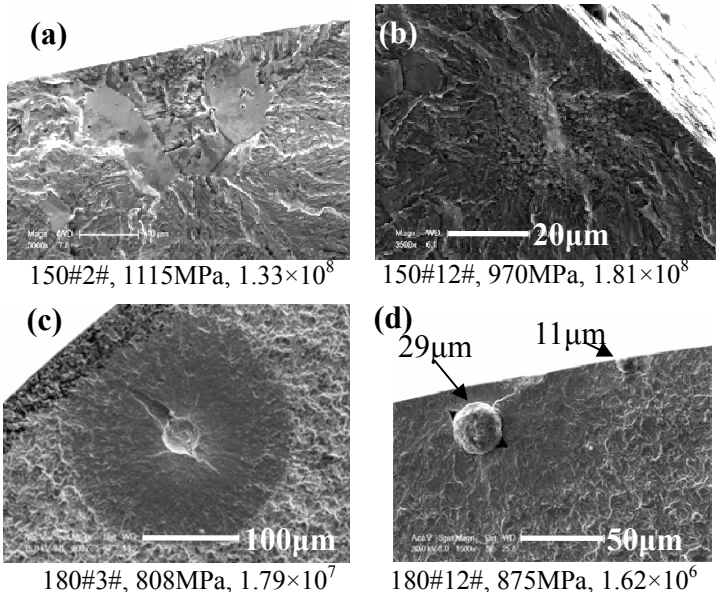

Fig. 5. Typical examples of fracture surface morphology for fatigue crack initiation. (a) interior grains boundary initiation for RL150, (b) interior grains boundary initiation with FGA for VHCF of RL150, (c) fisheye pattern with FGA for VHCF of RL180, and (d) competition between surface inclusion initiation and interior inclusion initiation.

Effects of microstructures on VHCF crack initiation are shown in Table 2. On one hand, VHCF crack tends to originate from interior grain boundary at low tempering temperature for RL150, while interior inclusion is prone to be the crack origin when the tempering temperature is up to 180℃ and 300℃. On the other hand, values of stress intensity factor of FGA: ΔK_{FGA} fluctuate around a constant for each of specimen group. ΔK_{FGA} reaches its highest value for RL180, and the lowest value for RL300. Retained austenite content is responsible for the change of ΔK_{FGA}, for the threshold value of crack growth ΔK_{th} varies with the volume fraction of retained austenite[14].

Table 2. Statistical Comparison of VHCF crack initiation for the three specimen groups

	Inclusion	Grain boundary	ΔK_{FGA} (MPa*m$^{0.5}$)		ΔK_{Inc} (MPa*m$^{0.5}$)	
			Mean value	Standard deviation	Mean value	Standard deviation
RL150	11% (1/9)	89% (8/9)	5.29	0.1	2.54	0.28
RL180	100% (9/9)	0 (0/9)	5.52	0.58	4.27	0.39
RL300	73% (8/11)	27% (3/11)	4.31	0.36	3.83	0.51

5. Microstructure sensitivity analysis

As we know, FGA consumes more than 90 percent of VHCF life[13], thus it is reasonable to take the fatigue life of FGA formation as the whole fatigue life. Based on the conclusion that FGA is finished when the plastic zone size r_p of the microcrack exceeds the low boundary width l_m of the martensite[17], this paper considers that the martensite is the key factor for the FGA formation for

high strength steel. During the formation of FGA, localized and irreversible plastic flows are blocked within the twin martensite, and fatigue crack occur with the fracture of martensite when the accumulated energy reaches the critical value. We assume that the dislocations are piled up along the slip band in the martensite, and introduce the influence of the strength of the material and the law of FGA formation on the VHCF crack initiation life, thus we have the modified Tanaka-Mura model for life prediction of FGA:

$$N_{FGA} \cdot \pi(\tau - \kappa)^2 l_m^{\,2} / G = C \cdot \sigma_b \cdot area_{FGA,net} \tag{1}$$

Where l_m is the width of martensite, σ_b is tensile strength of the material, $area_{FGA,net}$ is the area of FGA minus the area of inclusion, and C is a correction coefficient which shows the relationship between the strength of the martensite and tensile stress of material. Other parameters are same as Tanaka-Mura model[18]. With Von Misses yield criteria, Eq. [1] can be expressed as:

$$N_{FGA} = \frac{9CG\sigma_b}{2\pi l_m^{\,2}(\sigma - \sigma_D)^2}\left(\frac{16\Delta K_{FGA}^2}{\pi^2\sigma^4} - area_{Inc}\right) \tag{2}$$

In Eq. [2], σ_D is the fatigue limit. With Eq. [2], sampling-based sensitivity measures are performed with direct Monte-Carlo simulation[19; 20]. The bulk shear modulus G, correction coefficient C, martensite width l_m and fatigue limit σ_D are assumed to be deterministic variables with values of 79 GPa, 1, 575 nm and 600MPa respectively. local stress σ, ΔK_{FGA}, and inclusion size $\sqrt{area_{Inc}}$ are assumed to be random variables. The stress is normally distributed with a mean value of 750 MPa and a COV of 0.03. ΔK_{FGA} is a normal distribution with a mean value of 5.5 MPam$^{0.5}$ and a COV of 0.03. Inclusion size is Gumbel distributed with a mean value of 30 μm and a COV of 0.4.

The calculated results of sensitivity measures are shown in Fig. 6. Both sensitivity of mean value S_μ and sensitivity of standard deviation S_σ are dimensionless and appropriate for variable ranking, and they are defined as[21]:

$$S_{\mu_i} = \frac{\partial P_f / P_f}{\partial \mu_i / \sigma_i}, \qquad S_{\sigma_i} = \frac{\partial P_f / P_f}{\partial \sigma_i / \sigma_i} \tag{3}$$

P_f, μ_i and σ_i are respectively the probability of failure, mean value and standard deviation of a variable X_i.

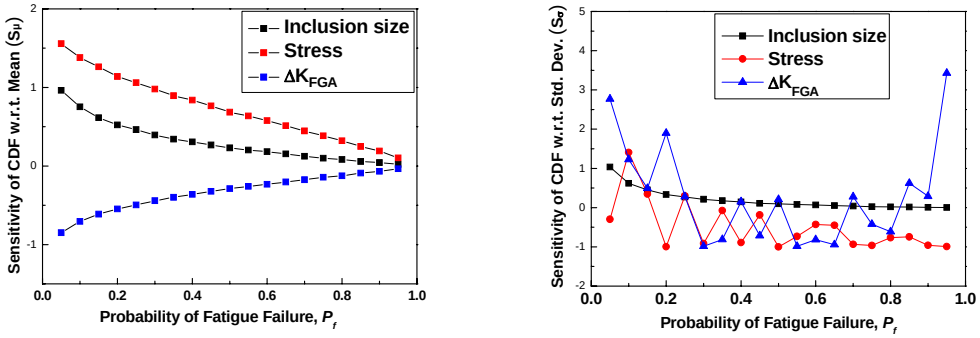

Fig. 6. (a) sensitivity of mean value (S_μ); (b) sensitivity of standard deviation (S_σ).

It is seen that fatigue failure being most sensitive to mean value of stress and standard deviation of ΔK_{FGA} by comparing the absolute value of S_μ and S_σ between these variables. Influence of mean value for the three variables does not appear to be much different from each other with the most sensitive variable of stress as shown in Fig. 6a. Mean value sensitivity of ΔK_{FGA} is close to that of inclusion size. Although inclusion size has an effect on life scatter by three orders when the stress is given[22], VHCF life with FGA has a much lower sensitivity of inclusion size under rotating bending as the stress gradient along the radius direction. Fig. 6b gives the sensitivity of standard deviation. As the probability of fatigue failure increased, standard deviation of stress and inclusion size have an decreasing influence on fatigue failure, while standard deviation sensitivity of ΔK_{FGA} is much higher than that of stress and inclusion size. For interior inclusion initiation, fatigue failure becomes more sensitive on ΔK_{FGA} deviation when the its mean value is obviously lower as the largest life scatter as RL300 shows.

6. Conclusions

A high carbon chrome steel was tempered at 150℃, 180℃, and 300℃, and VHCF test was performed with them. S-N curves show an increasing tendency of life scatter with the increasing of tempering temperature. In VHCF regime, interior inclusion initiation was dominant for RL180 and RL300 while interior grain boundary initiation was dominant for RL150 which has the highest volume fraction of retained austenite. FGA was observed in VHCF specimens, and ΔK_{FGA} is obviously lower for 300℃ with a large deviation of ΔK_{Inc}. A modified Tanaka-Mura model was proposed for the mechanism of FGA formation, and sensitivity measurements were carried out for microstructure variables ranking.

Acknowledgements

The authors gratefully acknowledge the support of the National Natural Science Foundation of China (Grant Nos. 11021262 and 11172304), and the National Basic Research Program of China (Grant No. 2012CB937500).

References

[1]T. Naito, H. Ueda, M. Kikuchi, Fatigue Behavior of Carburized Steel with Internal Oxides and Nonmartensitic Microstructure near the Surface. Metall Trans A, 15 (1984) 1431-1436.
[2]G.A. Qian, Y.S. Hong, Effects of Environmental Media on High Cycle and Very-High-Cycle Fatigue Behaviors of Structural Steel 40cr. Acta Metall Sin, 45 (2009) 1356-1363.
[3]G.A. Qian, C.E. Zhou, Y.S. Hong, Experimental and theoretical investigation of environmental media on very-high-cycle fatigue behavior for a structural steel. Acta Materialia, 59 (2011) 1321-1327.
[4]T. Sakai, B. Lian, M. Takeda, K. Shiozawa, N. Oguma, Y. Ochi, M. Nakajima, T. Nakamura, Statistical duplex S-N characteristics of high carbon chromium bearing steel in rotating bending in very high cycle regime. Int J Fatigue, 32 (2010) 497-504.
[5]J. Lai, T. Lund, K. Rydén, A. Gabelli, I. Strandell, The fatigue limit of bearing steels-Part I: A pragmatic approach to predict very high cycle fatigue strength. Int J Fatigue, 38 (2012) 155-168.
[6]M. Zimmermann, Diversity of damage evolution during cyclic loading at very high numbers of

cycles. Int Mater Reviews, 57 (2012) 73-91.
[7]A.G. Zhao, J.J. Xie, C.Q. Sun, Z.Q. Lei, Y.S. Hong, Effects of strength level and loading frequency on very-high-cycle fatigue behavior for a bearing steel. Int J Fatigue, 38 (2012) 46-56.
[8]D.L. McDowell, F.P.E. Dunne, Microstructure-sensitive computational modeling of fatigue crack formation. Int J Fatigue, 32 (2010) 1521-1542.
[9]K. Shiozawa, Y. Morii, S. Nishino, L. Lu, Subsurface crack initiation and propagation mechanism in high-strength steel in a very high cycle fatigue regime. Int J Fatigue, 28 (2006) 1521-1532.
[10]Y. Murakami, T. Nomoto, T. Ueda, Y. Murakami, On the mechanism of fatigue failure in the superlong life regime ($N>10^7$ cycles). Part I: influence of hydrogen trapped by inclusions. Fatigue Fract Eng Mater Struct, 23 (2000) 893-902.
[11]Y.B. Liu, Z.G. Yang, Y.D. Li, S.M. Chen, S.X. Li, W.J. Hui, Y.Q. Weng, Dependence of fatigue strength on inclusion size for high-strength steels in very high cycle fatigue regime. Mater Sci Eng A, 517 (2009) 180-184.
[12]S.X. Li, Effects of inclusions on very high cycle fatigue properties of high strength steels. Int Mater Reviews, 57 (2012) 92-114.
[13]Q.Y. Wang, C. Bathias, N. Kawagoishi, Q. Chen, Effect of inclusion on subsurface crack initiation and gigacycle fatigue strength. Int J Fatigue, 24 (2002) 1269-1274.
[14]R.O. Ritchie, V.A. Chang, N.E. Paton, Influence of Retained Austenite on Fatigue Crack-Propagation in Hp9-4-20 High-Strength Alloy-Steel. Fatigue Eng Mater Struct, 1 (1979) 107-121.
[15]D.Y. Wei, J.L. Gu, H.S. Fang, B.Z. Bai, Z.G. Yang, Fatigue behavior of 1500 MPa bainite/martensite duplex-phase high strength steel. Int J Fatigue, 26 (2004) 437-442.
[16]C.S. Lee, K.A. Lee, D.M. Li, S.J. Yoo, W.J. Nam, Microstructural influence on fatigue properties of a high-strength spring steel. Mater Sci Eng A, 241 (1998) 30-37.
[17]A.G. Zhao, J.J. Xie, C.Q. Sun, Z.Q. Lei, Y.S. Hong, Prediction of threshold value for FGA formation. Mat Sci Eng A, 528 (2011) 6872-6877.
[18]K. Tanaka, A Theory of Fatigue Crack Initiation at Inclusions. Metall Trans A, 13 (1982) 117-123.
[19]Y.T. Wu, S. Mohanty, Variable screening and ranking using sampling-based sensitivity measures. Reliab Eng Syst Saf, 91 (2006) 634-647.
[20]Z.Q. Lei, J.J. Xie, A.G. Zhao, Y.S. Hong, A simulation on microstructure sensitivity to very-high-cycle fatigue behavior of metallic materials. Procedia Eng, 4 (2010) 225-232.
[21]Y.T. Wu, S. Mohanty, Variable screening and ranking using sampling-based sensitivity measures. Reliab Eng Syst Saf, 91 (2006) 634-647.
[22]Z.Q. Lei, Y.S. Hong, J.J. Xie, C.Q. Sun, A.G. Zhao, Effects of inclusion size and location on very-high-cycle fatigue behavior for high strength steels. Mater Sci Eng A, 558 (2012) 234-241.